




Cite this: *RSC Adv.*, 2024, 14, 8905

Quinoline–sulfonamides as a multi-targeting neurotherapeutic for cognitive decline: *in vitro*, *in silico* studies and ADME evaluation of monoamine oxidases and cholinesterases inhibitors†

Saquiab Jalil,^{ab} Zahid Hussain,^a Syed Mobashir Ali Abid,^{ab} Abdul Hameed ^d and Jamshed Iqbal ^{*abc}

Alzheimer's disease (AD) is a multifactorial irreversible neurological disorder with multiple enzymes involved. In the treatment of AD, multifunctional agents targeting cholinesterase (ChE) and monoamine oxidase (MAO) inhibitors have shown promising results. Herein, a series of novel quinoline–sulfonamides (**a1**–**18**) were designed and synthesized as a dual inhibitor of MAOs and ChEs. The *in vitro* results showed that compounds **a5**, **a12**, **a11**, and **a6** exhibited the most potent compounds against specific enzymes. They had IC₅₀ value 0.59 ± 0.04 for MAO-A, 0.47 ± 0.03 for MAO-B, 0.58 ± 0.05 for BChE and 1.10 ± 0.77 for AChE μM respectively. Furthermore, kinetic studies revealed that these compounds are competitive. Molecular docking studies enhanced the understanding of the *in silico* component, unveiling critical interactions, specifically the hydrogen bonding interaction, π–π, π–alkyl, π–amid and π–sulfur interactions between the ligand and enzymes. These findings suggest that compounds **a5**, **a6**, **a11**, **a12**, **a15**, and **a18** may be potent multifunctional candidates for AD treatment.

Received 13th August 2023
Accepted 5th March 2024

DOI: 10.1039/d3ra05501a

rsc.li/rsc-advances

1 Introduction

Alzheimer's disease (AD) is a multifactorial neurodegenerative disease that causes abnormal behavior, impaired cognitive abilities such as learning, memory, perception, and problem-solving.^{1,2} The pathophysiology of the disease is quite complicated and two hypotheses have been proposed, such as “cholinergic” and “amyloid”. According to the Amyloid hypothesis, the hallmarks of AD include amyloid beta aggregates which lead to neural cells deaths.³ According to the second hypothesis, the cholinergic hypothesis, acetylcholine (ACh) is not produced in sufficient quantities in AD due to less production of a neurotransmitter that plays a significant role in sleep, learning, attention, and sensitivity.⁴ AD is caused by aberrant expression of cholinesterase's (acetylcholinesterase: AChE and butyrylcholinesterase: BChE) and monoamine oxidases (MAO-A and MAO-B).^{5,6} Inhibiting the enzyme can raise

the level of MAO and AChE in the presynaptic cleft and improve signaling.⁷

Monoamine oxidase (MAO) is an enzyme that regulates mood, emotions, and behavior. As a result of amines degradation, reactive oxygen species (ROS) and hydrogen peroxide (H₂O₂) were produced *via* Fenton reaction, which were responsible for neural cell death.⁸ Neurotransmitter deficiencies, can causes the neurodegenerative diseases, Alzheimer's, disease, Parkinson's disease and depression. Monoamine oxidase inhibitors (MAO-Is) play a crucial role in neurodegenerative diseases. By reducing the breakdown of neurotransmitters such as dopamine, serotonin, and noradrenaline in nerve endings, increases the level of monoamine oxidase. MAO-A inhibitors are primarily used to treat depression, while MAO-B inhibitors are commonly used to treat Alzheimer's, Parkinson's and other neurological diseases.⁹

Choline esterase is found in the central nervous system. It exists in two isoforms acetylcholinesterase (AChE EC 3.1.1.7) and butyrylcholinesterase (BChE EC 3.1.1.8) which are responsible for metabolizing AChE into acetic acid and choline, leads to neural cell death.¹⁰ Alzheimer's disease is characterized by decreased neurotransmitter levels, especially acetylcholine (ACh) in the brain. One of the most prominent biochemical changes in AD is the reduction in brain acetylcholine levels. Cholinergic inhibitors are used to inhibit and can increase AChE levels in the brain improve signaling.⁵ Different class of

^aDepartment of Pharmacy COMSATS University Islamabad, Centre for Advanced Drug Research, Abbottabad Campus, Abbottabad-22060, Pakistan. E-mail: drjamshed@ciit.net.pk; jamshediqb@googlemail.com

^bDepartment of Pharmacy, COMSATS University Islamabad, Abbottabad Campus, Abbottabad 22060, Pakistan

^cDepartment of Chemistry, COMSATS University Islamabad, Abbottabad Campus, Abbottabad 22060, Pakistan

^dDepartment of Chemistry, University of Sahiwal, Sahiwal, 57000, Pakistan

† Electronic supplementary information (ESI) available. See DOI: <https://doi.org/10.1039/d3ra05501a>



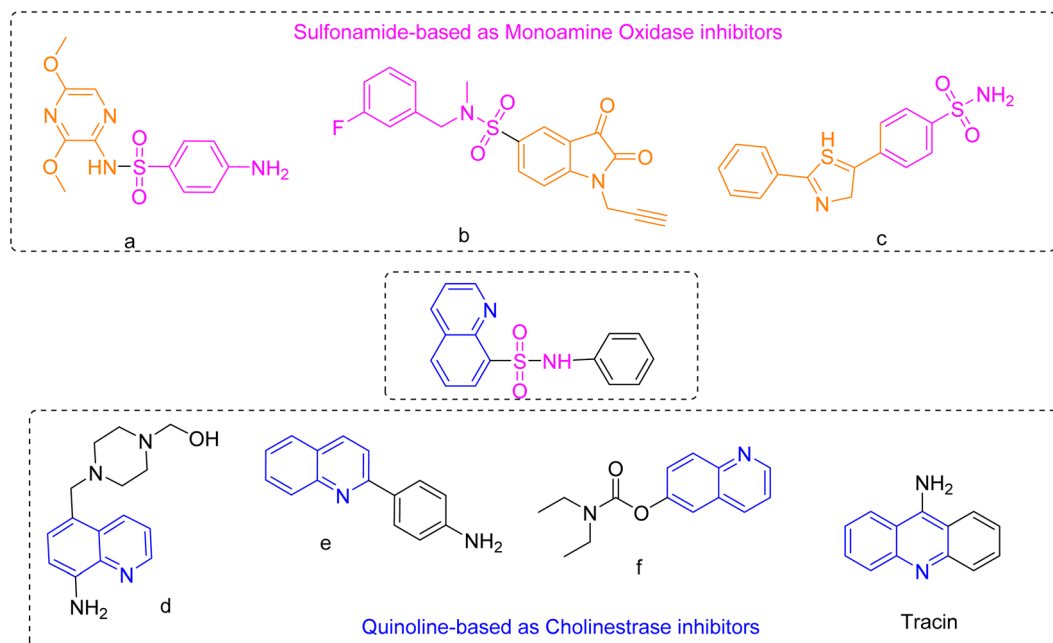


Fig. 1 Some similar derivatives containing quinoline and sulfonamide hybrids possessing anti-Alzheimer's activities.

compounds have been identified as a MAO and ChE inhibitors among them quinoline gain much attention.¹¹

The quinoline is a bicyclic chemical compound containing a pyridine ring fused to a benzene ring. This compound is found in several natural compounds (*Cinchona* alkaloids) and in drugs, with a wide range of biological effects, anti-malarial,¹² anti-bacterial,¹³ anti-fungal,¹⁴ anti-cancer,¹⁵ anti-convulsant,¹⁶ anti-inflammatory,¹⁷ neurodegenerative^{18,19} and analgesic activities.²⁰ Whereas, sulfonamide moiety has emerged as a prominent focus of research in recent years. Numerous review articles highlighting the significance of this nucleus is displaying a broad spectrum of biological activities. Various studies have shown that sulfonamide, when combined with heterocycles such as coumarin (a)²¹ isatin^{22,23} thiazole (c)²⁴ and quinoline (d, e and f),^{25,26} exhibit excellent anti-Alzheimer properties as shown in Fig. 1.

Herein we plan to introduce sulfonamide moiety into the quinoline skeleton to obtain novel quinoline-sulfonamide hybrids for MTDLs.

Presently, there is no cure for AD, but several treatments have been found that slow down the progression and ease the symptoms.²⁷ It is a well-known fact that monoamine oxidase and cholinesterase play critical roles in cognitive function and decline. Therefore, a more comprehensive approach that targets a variety of enzymes simultaneously is needed for complex diseases. Rather than traditionally treating one disease with only one drug, the concept of one drug, multiple targets has become commonplace. In recent years, multiple target drug ligands (MTDLs) have been developed, which are molecules that bind simultaneously to multiple enzymes (Fig. 2).^{28–30} Multi-target approaches can also reduce side effects and improve

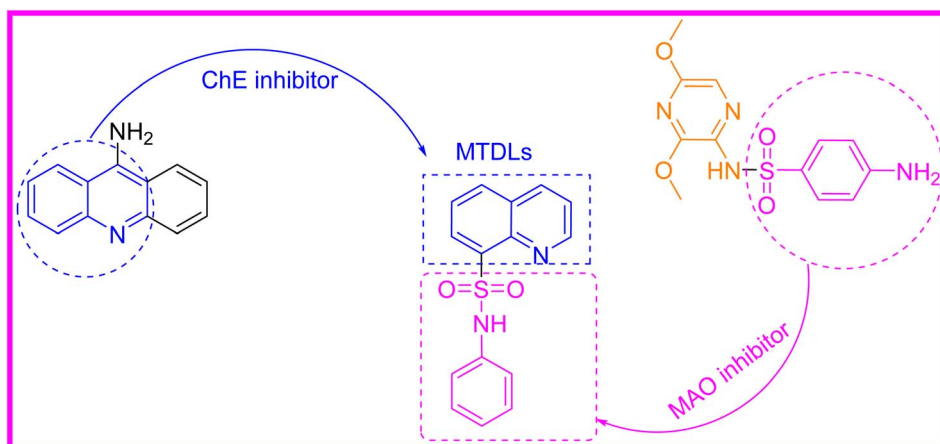


Fig. 2 Design strategy of quinoline-sulfonamide hybrids.



treatment outcomes. Few types of chemicals have been identified as MAO and ChEs inhibitors.³¹

In the present work, we have design and synthesized quinoline-sulfonamide derivatives and studied their biological non-selective potential against targeted enzymes. Kinetic studies have been used to determine the mode of inhibition of potent compounds. The compound was also explored *in silico* for its interactions with different amino acids residues at the catalytic site.

2 Results and discussion

2.1. Chemistry

2.1.1 General procedure for the synthesis of quinoline-8-sulfonamide. The quinoline-8-sulfonamide derivatives were synthesized. We dissolved quinoline-8-sulfonyl chloride (200 mg, 1 mM) in dichloromethane and stirred for 1 h. The temperature was decreased to 10 °C, then substituted amines (100 µL, 1 mM) was added, followed by addition of pyridine (1–2 drops). Reaction progress was monitored by thin layer chromatography (TLC) and a stirrer overnight, until the final product was obtained. Upon completion of the reaction, the reaction mixture was poured into

a beaker with cold distilled water, 2–3 drops of concentrated HCl were added, and a precipitate was formed. The synthesized compounds (**a1–18**) were obtained in excellent yields (80–90%). The structures were confirmed through ¹H NMR, ¹³CNMR, and FT-IR spectroscopic techniques.

2.2. Biological activity

The compounds were investigated for inhibition of MAOs and ChEs. Enzyme inhibition assays of reference and test compounds on MAO (MAO-A and MAO-B) and ChE (AChE and BChE) were performed. Positive controls included clorgyline for MAO-A and deprenyl for MAO-B, as well as Donepezil for AChE and BChE. IC₅₀ values for newly synthesized compounds and reference inhibitors are summarized in Table 1. General structure of quinoline-8-sulfonamide were present in Fig. 3.

2.3. Enzyme inhibition structure–activity relationship analysis

The structure of a compound can be systematically modulated to investigate the effect of different functional groups or modifications on its activity *in vitro*. A remarkable inhibitory effect was observed on the newly synthesized hybrids. The

Table 1 IC₅₀ values of synthesized compounds against monoamine oxidases and choline esterase

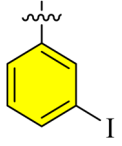
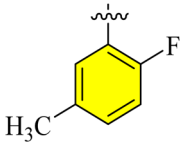
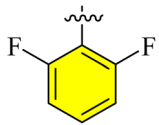

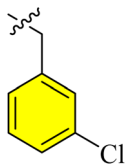
Codes	R'	IC ₅₀ ^a (µM)			
		MAO-A	MAO-B	AChE	BChE
a1		1.17 ± 0.77	2.73 ± 0.16	1.11 ± 0.57	N/A ^b
a2		2.74 ± 1.09	1.81 ± 0.98	2.58 ± 0.97	N/A
a3		0.61 ± 0.04	1.69 ± 0.16	1.01 ± 0.59	N/A
a4		0.78 ± 0.03	2.29 ± 0.50	2.18 ± 1.17	N/A
a5		0.59 ± 0.04	0.73 ± 0.08	1.95 ± 1.07	2.84 ± 1.07

Table 1 (Contd.)

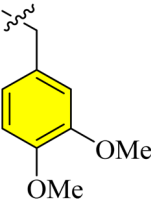



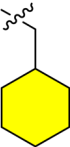
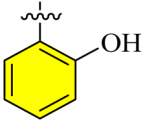

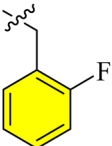
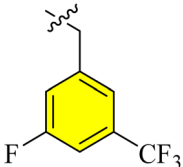
Codes	R'	IC ₅₀ ^a (μM)			
		MAO-A	MAO-B	AChE	BChE
a6		2.34 ± 0.91	1.07 ± 0.65	1.11 ± 0.47	1.10 ± 0.89
a7		2.45 ± 1.01	2.23 ± 1.08	1.73 ± 0.87	N/A
a8		2.75 ± 0.79	1.26 ± 0.98	1.15 ± 0.72	N/A
a9		2.25 ± 0.94	1.20 ± 0.45	3.78 ± 0.92	N/A
a10		2.44 ± 0.98	2.26 ± 1.12	1.36 ± 0.77	N/A
a11		1.25 ± 0.45	1.09 ± 0.65	0.58 ± 0.05	1.72 ± 0.68
a12		1.34 ± 0.67	0.47 ± 0.03	2.65 ± 0.97	1.16 ± 0.77
a13		1.04 ± 0.67	1.22 ± 0.99	1.65 ± 0.97	N/A
a14		2.58 ± 1.23	0.91 ± 0.08	3.06 ± 0.77	1.176 ± 0.57



Table 1 (Contd.)

Codes	R'	IC ₅₀ ^a (μM)			
		MAO-A	MAO-B	AChE	BChE
a15		1.16 ± 0.49	1.20 ± 0.50	1.40 ± 0.54	N/A
a16		1.92 ± 0.76	1.48 ± 0.76	1.92 ± 0.87	N/A
a17		2.59 ± 1.10	1.79 ± 0.88	2.34 ± 0.67	N/A
a18		1.03 ± 0.56	2.22 ± 0.99	1.01 ± 0.61	2.784 ± 0.92
Clorgyline ^c		0.045 ± 0.03	61.35 ± 1.13	—	—
Deprenyl ^c		67.25 ± 1.02	0.0196 ± 0.001	—	—
Donepezil ^c		—	—	0.032 ± 0.003	6.41 ± 0.34

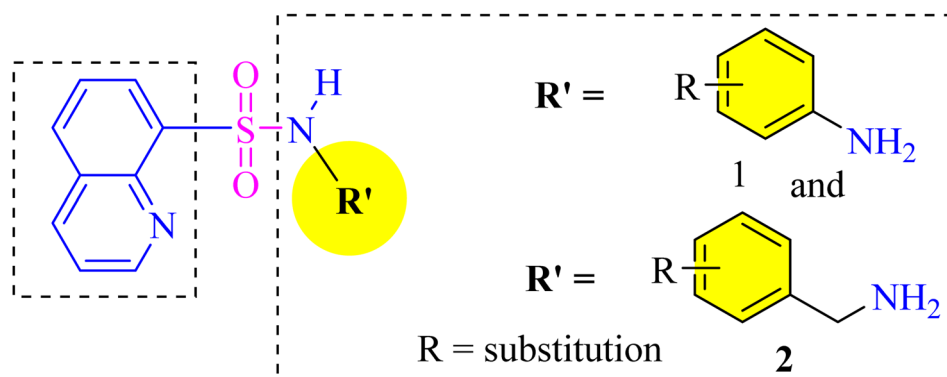
^a IC₅₀ (μM). ^b Not active. ^c Standard inhibitors.

Fig. 3 General structure of phenyl/benzyl-quinoline-8-sulfonamide.

benzyl group substituents are responsible for the differential inhibition activities observed in these compounds.²⁶ All synthetic analogues showed variable results in IC₅₀ = 0.59 ± 0.04 to 2.85 ± 1.09 μM for MAO-A and 0.47 ± 0.03 to 2.73 ± 0.16 μM for MAO-B. The introduction of the electro-withdrawn group

(EWG) and electron donating group (EDG) to the phenyl ring resulted in a substantial inhibitory effect.

Chloro substitution at *meta* (*m*-), *ortho* (*o*-) and *para* (*p*-) position affects the compound's inhibition potential against selected targets. *Meta* substitution is the most active



substitution. As a result of di-chloro substitution, *o*- and *p*-substituted compounds have a lower inhibition potential (**a15**). Furthermore, when di-substitution at *o*- and *m*- with chlorine and *p*-hydroxyl, the potency also decreased 4-fold on the same enzyme. When chlorine is replaced by fluorine, the di-fluoro substitution at the *o*-position makes it more potent toward the enzyme, but its activity is less than *m*-chloro. When there is di-substitution at *o*- and *p*- (**a12** and **a13**), its activity was nearly the same and decreased 2-fold compared to (**a3**), also the activity of (**a14**) and (**a2**) dropped 4-fold. Replacing chlorine with *m*-iodine (**a1**) results in low potency, whereas changes in position from *meta* to *para* (**a8**) result in a 2-fold decrease in potency with respect to the *m*-position. The potency of the compounds is also affected when the halogen is replaced by other functional groups, such as methoxy. The *m*-substitution of methoxy (**a18**) was 2-fold more potent than di-substitution (**a6**), indicating that di-substitution decreases the potency of the targeted enzyme. The introduction of *m*-cyano (**a9**), benzimidazole ring (**a7**), and hexane ring (**a10**) resulted in almost the same potency. Results are summarized in Table 1.

The compound featuring *o*-fluoro substitution (**a12**) demonstrated the highest potency against MAO-B, while the di-substituted compound (**a14**) exhibited nearly equivalent efficacy. Notably, altering the position from *ortho* to *para* (**a13**) led to a 3-fold reduction in potency. Di-substitutions of phenyl rings (**a2** and **a3**) resulted in a substantial 4-fold decrease in potency.

Intriguingly, replacing fluorine with chlorine revealed interesting behavior, with *m*-chloro substitution yielding almost the same potency as (**a12**). Similarly, transitioning from *m*-chloro (**a5**) to *o*-chloro (**a16**) resulted in a 2-fold potency decrease, while the shift to *p*-chloro (**a15**) led to a 3-fold decrease. Moreover, di-substitutions (**a15** and **a17**) resulted in a nearly 2-fold decrement in potency.

In comparison, substituting *p*-iodine (**a8**) resulted in a compound that is 3-times less potent than (**a12**), while a shift from *p*-iodine to *m*-iodine (**a1**) caused a two-folds reduction in potency. Additionally, *p*-methoxy substitution (**a18**) exhibited nearly 2.5-fold lower potency compared to di-substitution (**a6**). Minimal distinctions were observed among the outcomes of compounds (**a7**), (**a9**), (**a11**), and (**a10**), all demonstrating a potency 2-fold less than the most potent compound (**a12**). These findings are summarized in Table 1.

Similarly, introducing *o*-hydroxy (**a11**) enhanced potency against AChE. However, substituting *o*-hydroxy with *o*-chloro (**a16**), *m*-chloro (**a5**), and *p*-chloro (**a4**) resulted in an approximate 4-fold decrease in activity compared to (**a11**). Furthermore, compound (**a15**) exhibited almost 2.5-fold less potency than (**a11**). The introduction of hydroxyl groups in di-chloro (**a17**) led to a substantial 5-fold decrease in substitution activity, underscoring that mono-substitution (**a11**) is the most favorable configuration. In summary, these observations emphasize the crucial role of specific substitutions in determining the efficacy

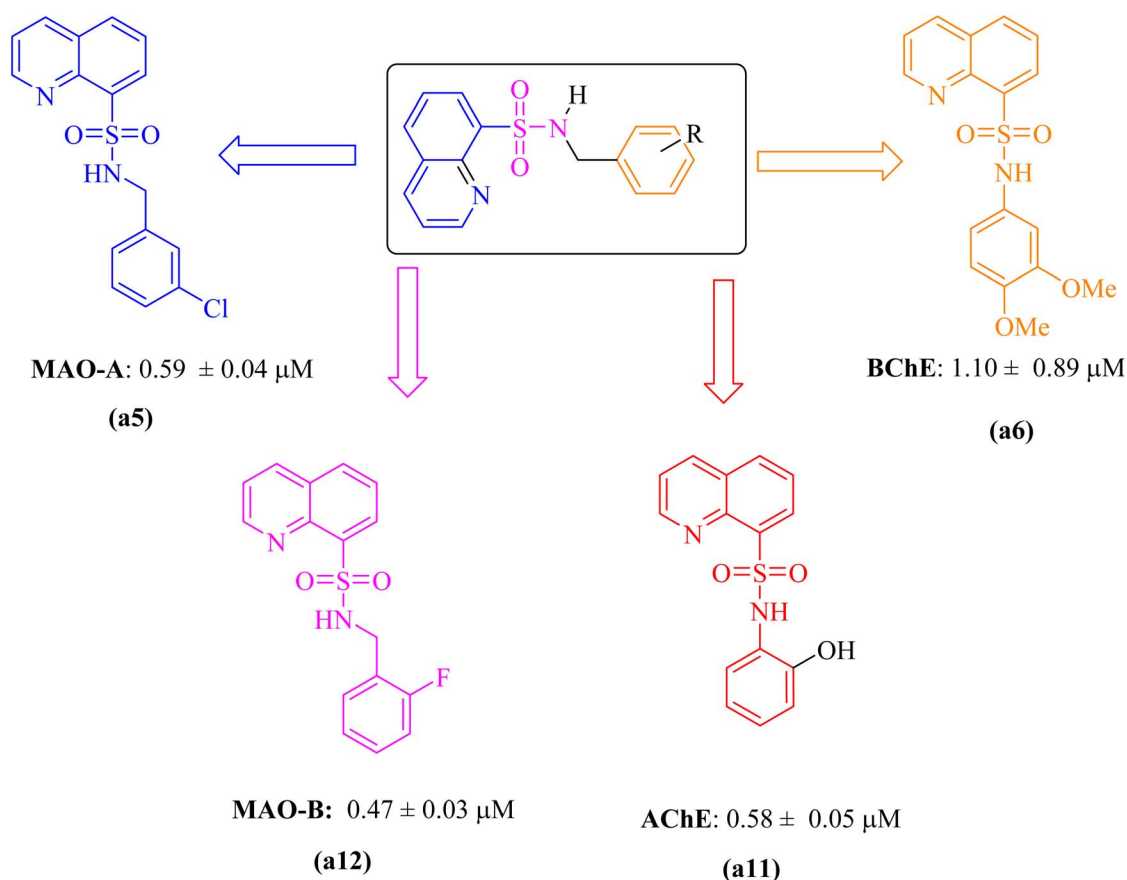


Fig. 4 Most potent inhibitor of MAO-A, MAO-B, AChE and, BChE.



of compounds against AChE, with mono-substitution at *o*-hydroxy position proving to be the most favorable. Replacing chloro with fluoro had a notable impact on compound potency. Compound (**a13**) showed a 3-fold decrease compared to the most potent, while positional changes further diminished activity. Compounds (**a3** and **a2**) were nearly 3-fold less active than (**a11**). Substituting fluoro with iodio (**a1** and **a8**) yielded compounds with similar, albeit almost 2-fold less, potency than the most potent compound. Halogen substitution with methoxy (**a18** and **a6**) resulted in compounds 2-fold less potent than (**a11**). Compound (**a9**) exhibited a significant 7-fold potency decrease. BChE inhibition revealed di-methoxy substitution (**a5**) as more potent, though activity decreased 2-fold with mono-substitution (**a18**). Compound (**a14**) matched (**a5**) in potency, but (**a5**) showed almost 2-fold less activity. These findings, detailed in Table 1.

2.4. Potent inhibitor against targeted enzymes

Potency of the compounds depends upon the structural confirmation and position of the substituent attached with them in the given series the most potent inhibitor was

illustrated in the Fig. 4. Compound (**a5**) showed more potency towards MAO-A having chloro group at *m*-position and compound (**a12**) showed more potency towards MOA-B due to presence of fluoro group at *o*-position same pattern was also observed in case of AChE and BChE but the substituent were different the potent inhibitor (**a6**) against BChE contain *o*-, *m*-methoxy ($-\text{OCH}_3$) groups and compound (**a11**) against AChE contain hydroxyl (OH) group at *o*-position the results shows that both *ortho* and *meta* position play important role in the inhibition of the targeted enzymes.

2.5. Enzyme kinetic studies

Kinetic studies of the most potent inhibitors were conducted to find the modes of inhibition against MAO-A, MAO-B, AChE, and BChE. The most potent inhibitors were tested at different concentrations. Several concentrations of compound *vs.* substrate were used to determine the mode of inhibition. Different concentrations of compounds **a5** (0.500, 0.600, 0.700, 0.800 μM), **a12** (0.500, 0.600, 0.700, 0.800 μM), **a11** (0.10, 0.20, 0.30, 0.40 μM) and **a6** (0.60, 0.80, 1, 1.20, 1.40 μM) and substrates (*p*-tyramine) (0.75, 1.5, 3, 4.5 and 6 mM), ATCII (1.25,

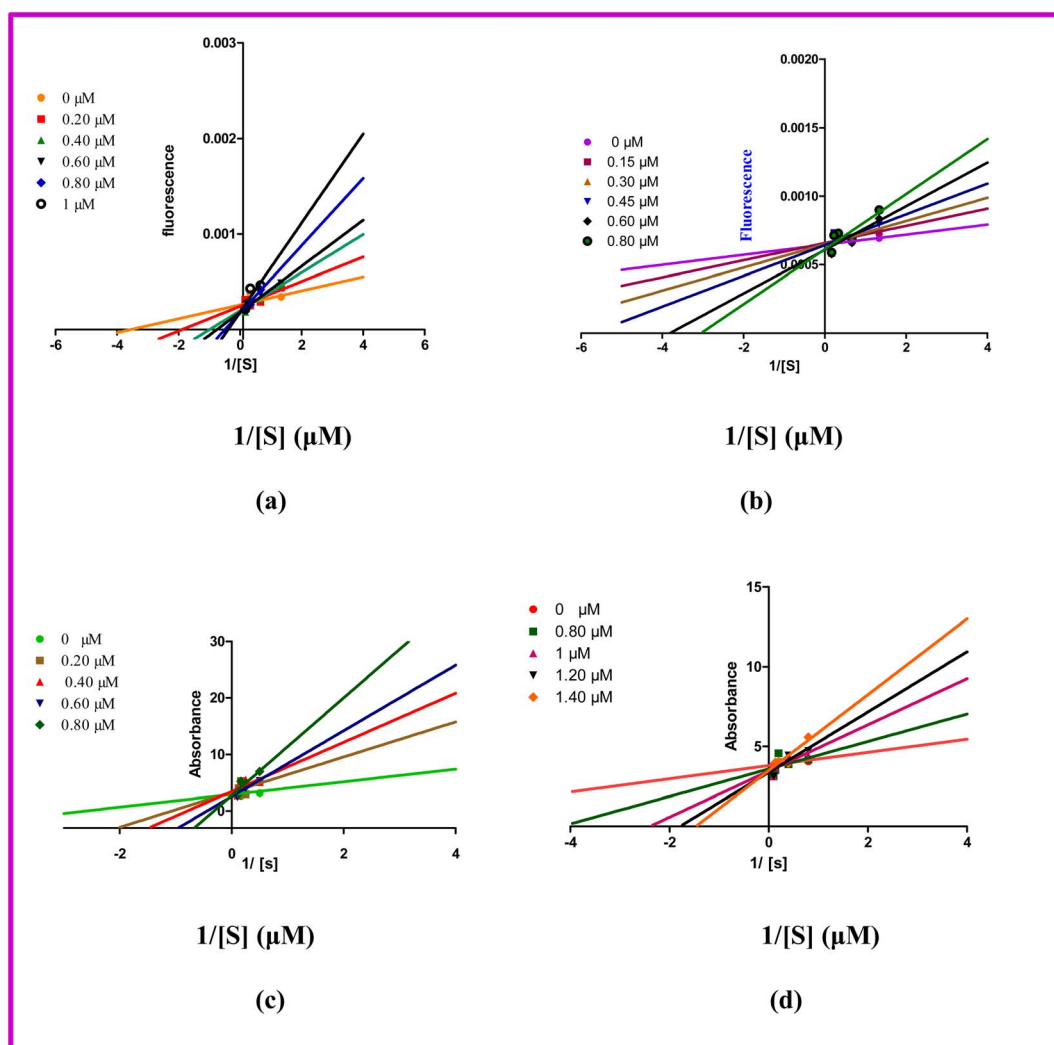


Fig. 5 Double reciprocal plot of MAO-A (a), MAO-B (b), AChE (c), and BChE (d) by compound **a5**, **a12**, **a11**, and **a6** respectively.

2.5, 5, 7.5, and 10 mM), and BTCII (1.25, 2.5, 5, 7.5, and 10 mM) were used to perform the assay as previously reported method.²⁶ Line Weaver–Burk graphs were used to analyze the inhibitory effect and determine the type of inhibition. All the tested compounds (**a5**, **a12**, **a11**, **a6**) showed competitive inhibition toward MAO-A, MAO-B, AChE and BChE respectively as displayed in Fig. 5.

2.6. Molecular docking studies

2.6.1 Monoamine oxidase (MAO-A and MAO-B). Molecular docking studies were performed on human MAO-A (PDB ID: 2Z5Y) and MAO-B (PDB ID: 2V5Z), as well as acetylcholinesterase (PDB ID: 1EVE) and butyrylcholinesterase (PDB ID: 4BDS). The results of *in vitro* inhibition of monoamine oxidase and cholinesterase were further explained by inhibitor interaction with the enzyme's active site. Monoamine oxidase's

active site has three functional domains. These were the entrance cavity, the substrate cavity and the third the aromatic cage (formed from Tyr398, Tyr435 and FAD).³² Cognate ligand (harmin) was docked within MAO-A's active pocket and an RMSD of 1.3 Å was obtained, before docking the potent compounds. The most potent compound **a5** was docked within the active pocket and the Hydrogen bonding form between the oxygen of sulfonamide with the TYR69 and ALA68 with a bond distance of 3.23 Å and 2.92 Å and binding energy -10.40 kcal mol⁻¹. Phenyl ring and quinoline ring displayed π - π , π -alkyl and π -amide interaction the amino acid TYR407, MET445 and GLY66 separately. The hydrophobic interactions between the aromatic rings and the amino acids also stabilize the enzyme's structure. This ensures the enzyme's active conformation is maintained for efficient substrate binding and catalysis. Chlorine at the *meta* position on the phenyl ring made alkyl interaction with the ILE335 and PHE352 amino acids

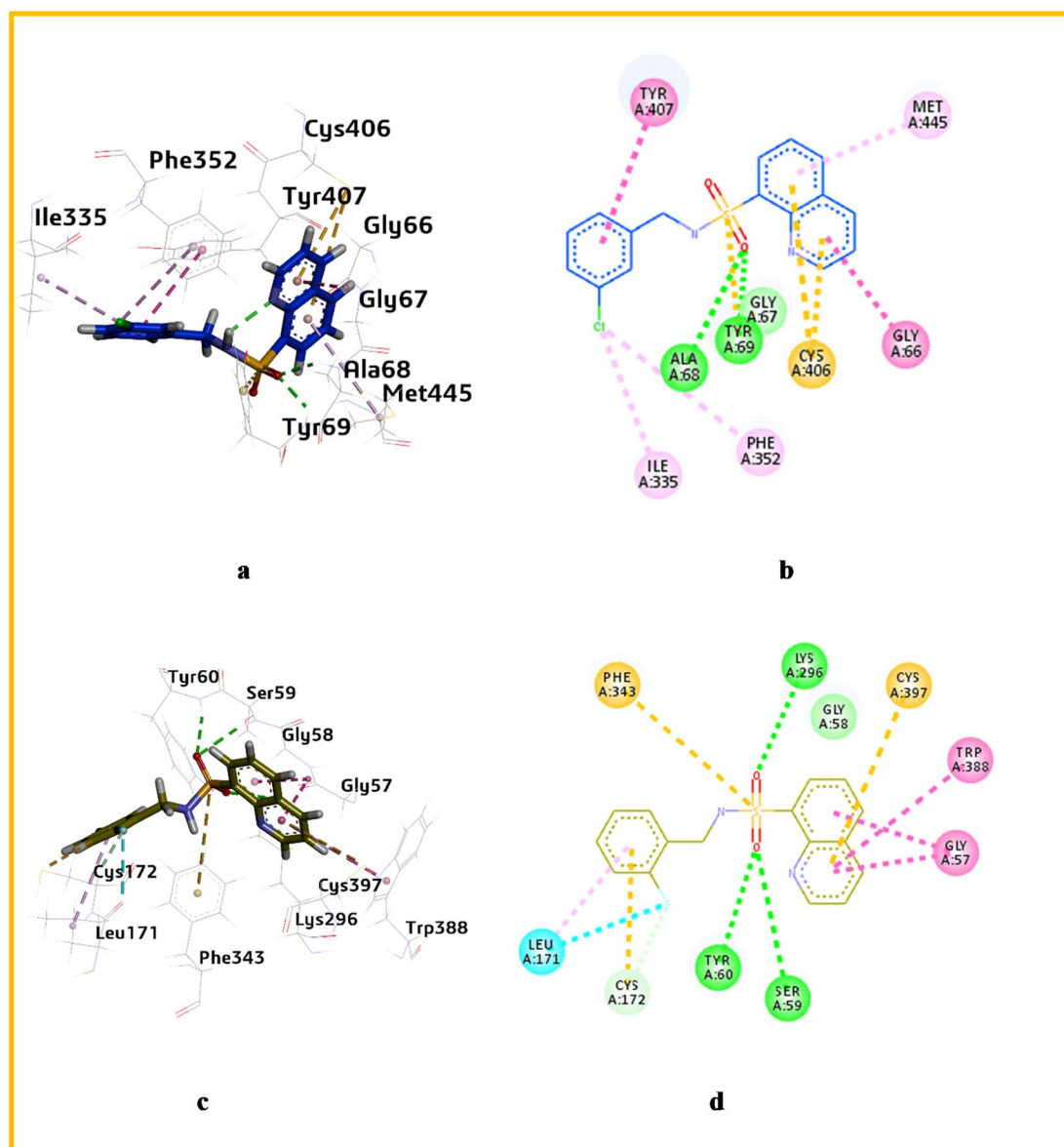


Fig. 6 3D and 2D interaction of compound **a5** MAO-A (a and b) and **a12** MAO-B (c and d).



residues, π -sulfur interaction was observed between the sulfur of sulfonamide and quinoline ring with the TYR69 and CYS406 amino acids respectively as shown in Fig. 6.

Similarly, prior to docking the potent compounds, a cognate ligand (safinamide) was docked within MAO-B's active pocket, and an RMSD 1.5 Å was obtained. Several interactions were observed between catalytic site amino acids and the most potent compound **a12**. Hydrogen bonding interaction was also observed between the sulfonamide oxygen and the amino acids TYR60, SER59 and ILY296 with a bond distance of 2.98 Å, 2.90 Å and 3.10 Å respectively, with binding energy -10.57 kcal mol $^{-1}$. Additionally, carbon-hydrogen bonds were found between fluorine and CYS172. This bond is also strong due to the electronegativity of the fluorine atom, which is higher than that of the carbon atom. Finally, π -alkyl and π - π interactions were present between the phenyl ring and quinoline ring with the amino acids LEU 171, and TRP 388. This interaction is possible due to the aromaticity of the rings, allowing them to form strong π -bonds with the amino acids as shown in Fig. 6.

The quinoline derivatives used in this study form strong interactions with enzyme active sites, resulting in adducts with

increased stability and activity. The majority of derivative molecules form H-bonds with MAO-A's TYR444 and TYR69. In the catalytic mechanism of MAO-A, TYR444 and TYR69 are involved. The quinoline compounds **a3**, **a5**, **a6** and, and **a8** form H-bonds with amino acids. The binding energy of compound **a6** was the highest, -10.40 kcal mol $^{-1}$.

All quinoline derivatives have an active interaction with enzyme active sites. The interactions were predominantly hydrophobic and van der Waals in nature. Hydrogen bonds have been formed in most derivative molecules with TYR434 and TYR60, involved in the catalytic mechanism of the MAO-B. It has been observed that compounds **a2**, **a18**, **a3**, **a4**, **a17**, **a5**, **a12**, **a6**, **a9**, and **a10** form H-bond with LEU171, GLY434, 435, and TYR60, amino acid residues play a key role in catalytic site. The binding energy of compound **a4** was the highest, -10.57 kcal mol $^{-1}$.

2.6.2 Choline esterase (AChE and BChE). Cognate ligand was docked within AChE's active pocket and an RMSD value 1.3 Å, was obtained, before docking the potent compounds. Several interactions were observed between the cognate ligand and the enzyme's active site. Hydrogen bonding interactions are highly

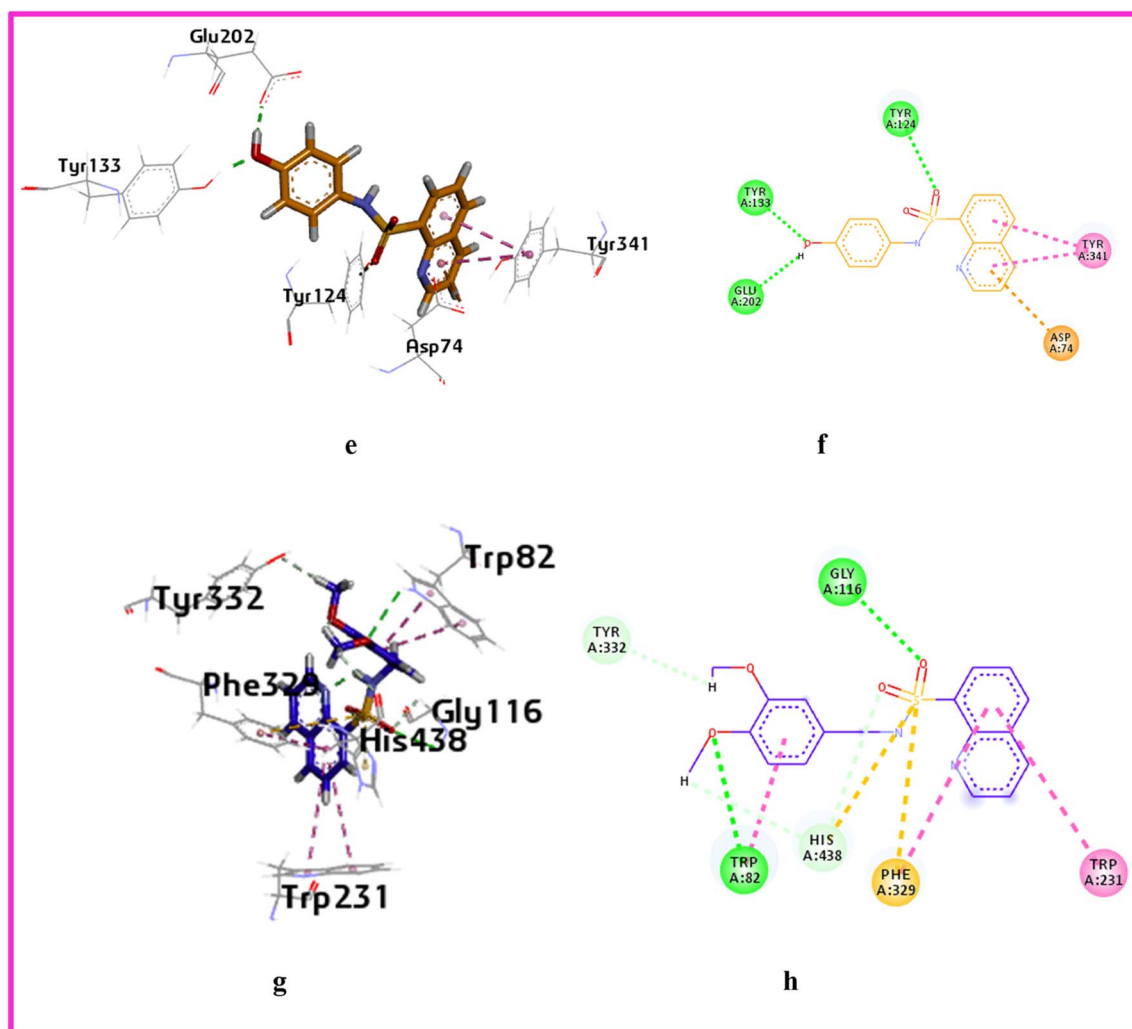


Fig. 7 3D and 2D interaction of compound **a11** left side AChE (e and f) and **a6** right side BChE (g and h).

Table 2 *In silico* ADME evaluation of synthesized compounds (a1–18)

Molecule	TPSA ^a	Lipinski violations	PAINS ^b	WLOGP ^c	HBA ^d	HBD ^e	GI absorption	BBB ^f permeant	NRB ^g
a1	67.44	0	0	4.25	4	1	High	Yes	4
a2	67.44	0	0	4.81	5	1	High	Yes	4
a3	67.44	0	0	5.04	5	1	High	No	3
a4	67.44	0	0	4.3	4	1	High	Yes	4
a5	67.44	0	0	4.3	4	1	High	Yes	4
a6	85.9	0	0	3.66	6	1	High	No	6
a7	91.5	0	0	2.27	4	3	High	No	3
a8	67.44	0	0	3.7	4	1	High	Yes	4
a9	67.44	0	0	4.25	4	1	High	Yes	4
a10	67.44	0	0	4.17	4	1	High	Yes	4
a11	87.67	0	0	3.35	5	2	High	No	4
a12	67.44	0	0	4.2	5	1	High	Yes	4
a13	67.44	0	0	4.2	5	1	High	Yes	4
a14	67.44	0	0	6.37	8	1	High	No	5
a15	67.44	0	0	4.95	4	1	High	Yes	4
a16	67.44	0	0	4.3	4	1	High	Yes	4
a17	76.67	0	0	3.65	5	1	High	Yes	5
a18	76.67	0	0	3.65	5	1	High	Yes	5

^a Topological polar surface area. ^b Pan-assay interference. ^c Logarithm of partition coefficient between *n*-octanol and water. ^d Hydrogen bond acceptor. ^e Hydrogen bond donor. ^f Blood–brain barrier. ^g Number of rotatable bonds.

stable and strong due to the electrostatic attraction between the partial positive hydrogen atom and the partial negative atoms of oxygen or nitrogen. This clearly indicates that OH at its *para*-position and oxygen of sulfonamide exhibit interactions with the amino acids TYR133, GLU202 and TYR124 with distances 2.86 Å, 3.30 Å and 3.01 Å respectively, with binding energy

−8.88 kcal mol^{−1}. In addition, the quinoline ring is seen to have a π -anion and π - π interaction with amino acids TYR 341 and ASP74. These interactions between the OH group and the sulfonamide oxygen, as well as the quinoline ring and the amino acids, further increase the strength of the hydrogen

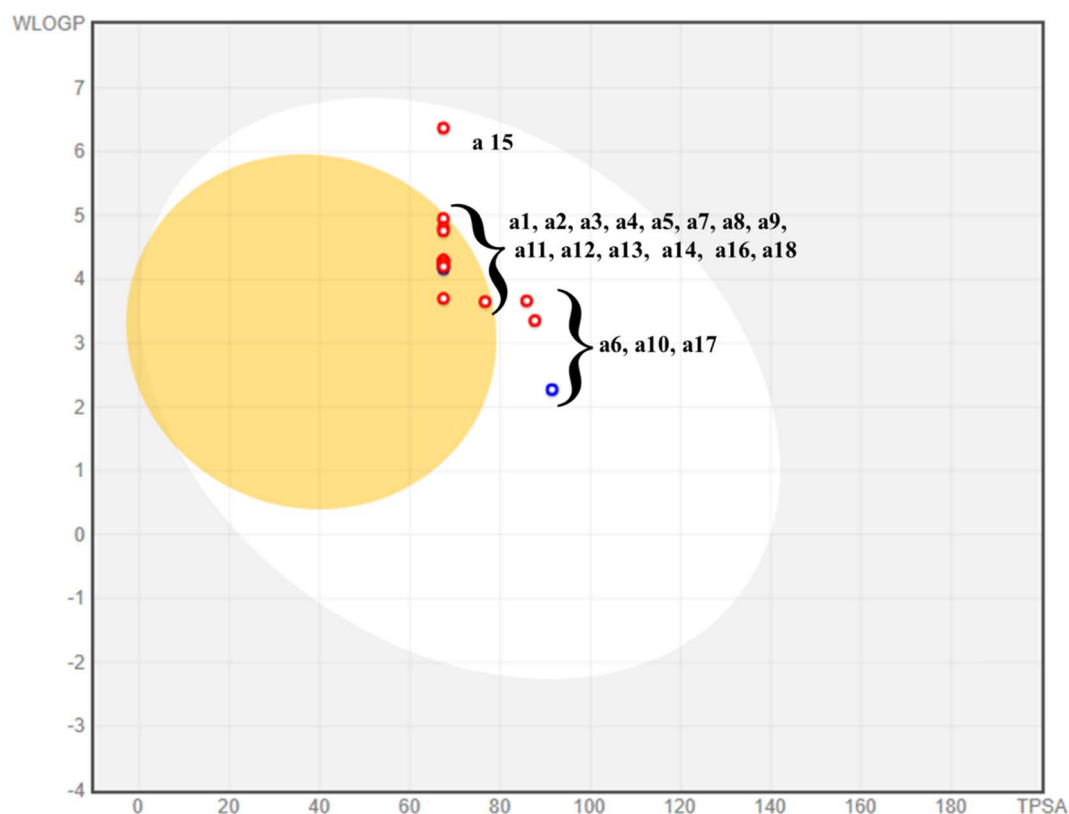


Fig. 8 The boiled-egg plot of the synthesized derivatives (a1–18).



bonding interaction. They contribute to the molecule's stability as shown in Fig. 7.

On the other hand, compound **a11** showed hydrogen bonding interactions between the oxygen atom and the sulfonamide with the amino acids TRP82 and GLY116 with distances 2.86 Å, 2.99 Å respectively, with binding energy -7.68 kcal mol $^{-1}$. Furthermore, a carbon hydrogen bond was observed between the hydrogen of methoxy and the oxygen of the sulfonamide with the amino acids TYR332 and HIS 438. Lastly, a π -sulfur interaction was seen between the sulfur of the sulfonamide and the amino acid PHE329 as shown in Fig. 7.

Several compounds formed hydrogen bonds with amino acid residues involved in the catalytic mechanism of the AChE enzyme. Among them **a1**, **a5**, **a10**, **a12**, **a15**, and **a16** formed hydrogen bonds with PHE 338 residue. The binding score of compound **a11** is highest, -8.68 kcal mol $^{-1}$.

2.7. Pharmacokinetic studies

Many predicted enzyme inhibitors are unable to proceed to the clinical trial stage due to their undesirable pharmacokinetic characteristics. Therefore, *in silico* approaches provide a reliable substitute for trials in earlier phases of studying a compound's fundamental pharmacokinetic features, and it's a sensible strategy to cut both the labor and associated costs. Using a web-based SwissADME, the absorption, distribution, metabolism, and excretion (ADME) profile of the produced compounds (**a1–18**) was developed. The results are described in Table 2. The boiled egg plot included in SwissADME is a quick, simple, and incredibly reliable way to predict a compound's passive gastrointestinal absorption.³³ The egg-shaped plot offers a visual summary of gastrointestinal absorption; it is represented by the white portion of the egg and the BBB penetration of the compound; it is shown as the inner yolk-like component of the egg and presents the boiled-egg plot of the recently synthesized derivatives as shown in Fig. 8.³⁴ The majority of the synthetic analogues exhibits brain penetration, as is shown from the plot. All compounds have the ability to penetrate the gastrointestinal tract and the BBB. The SWISSADME website generated the plot.³³ Every scaffold complied with Lipinski's law of drug resemblance.³⁵ Furthermore, the PAINS (Panassay Interference Compounds) filter was used to evaluate the promiscuity of the prepared hits. According to the data, each substance is distinct and does not share any chemical properties with the PAINS.³⁶ The topological polar surface area of all

the compounds ranged from 87 Å to 67 Å, and they all showed good gastrointestinal absorption. All of these factors indicate that synthetic hits could be promising treatments for the treatment of severe neurological diseases including Parkinson's and Alzheimer's.

3 Material and methods

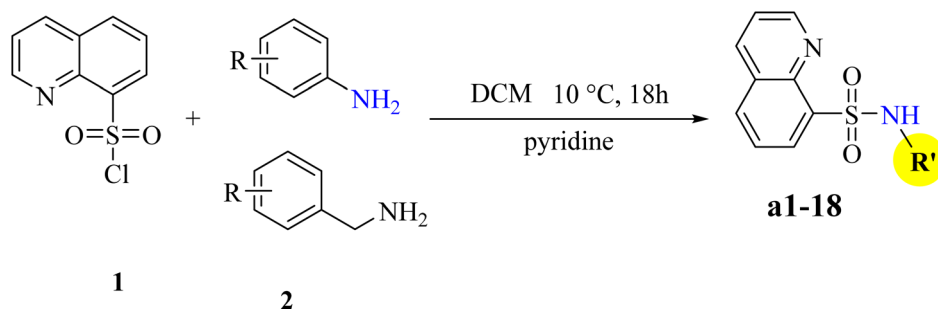
All the chemicals were purchased from Merck and Sigma-Aldrich (Steinheim, Germany). The thin layer chromatography (TLC) was used with pre-coated silica gel plates Keisel 60. The Bruker Advance NMR instrument (400 MHz) was used to measure ^1H and ^{13}C NMR in DMSO- d_6 . Chemical shift in with respect to tetramethylsilane as a reference compound was used and data reported in parts-per-million. Moreover, FTIR spectra was obtained on an Agilent Technology 630. Open capillary method (Gallenkamp melting point apparatus) was used to measure the melting point.

3.1. Experimental data

The synthesis of quinoline-8-sulfonamide derivative (**a1–18**) were discussed in Scheme 1.

3.1.1 N-(3-Iodophenyl)quinoline-8-sulfonamide (a1). Yield 91%, light brown powder, R_f : 0.4, (*n*-hexane/ethyl acetate: 2 : 3), M.P: 250–252 °C, FTIR (ν cm $^{-1}$), 3202 (stretching, NH), 1604 (stretching C=C), 1348 (S=O, stretching), 681 (C-I, stretching) cm $^{-1}$. ^1H NMR (400 MHz, DMSO- d_6) δ_{H} 9.11 (Ar-H, dd, $J = 4.0, 1.8$ Hz, 1H), 9.02 (NH, 1H, brs), 8.57 (Ar-H, dd, $J = 8.0, 1.8$ Hz, 1H), 8.37–8.30 (Ar-H, 2H, m), 7.79–7.69 (Ar-H, 3H, m), 7.18 (Ar-H, app td, $J = 8.0, 4.0$ Hz, 1H), 7.11 (Ar-H, dd, $J = 8.0, 4.0$ Hz, 1H), 6.81 (Ar-H, td, $J = 8.0, 1.8$ Hz, 1H). ^{13}C NMR (100 MHz, DMSO) δ_{C} 152.2 (C), 142.8, 139.9, 138.9, 137.7, 135.8, 134.9, 131.7, 129.5, 129.0, 127.5, 126.2, 123.3, 122.7, 94.8 (Ar-C). Anal. calculated for $\text{C}_{15}\text{H}_{11}\text{IN}_2\text{O}_2\text{S}$, %: C, 43.92; H, 2.70; N, 6.83; found, %: C, 43.81; H, 2.66; N, 6.85.

3.1.2 N-(2-Fluoro-5-methylphenyl)quinoline-8-sulfonamide (a2). Yield 89%, dark brown powder, R_f : 0.5, (*n*-hexane/ethyl acetate: 2 : 3), M.P: 260–262 °C, FTIR (ν cm $^{-1}$), 3288 (stretching, NH), 1636 (C=C, stretching), 1348 (stretching S=O), 642 (stretching, C-I) cm $^{-1}$. ^1H NMR (400 MHz, DMSO- d_6) δ_{H} 9.42 (1H, NH, brs), 9.12 (Ar-H, dd, $J = 4.0, 1.6$ Hz, 1H), 8.57 (Ar-H, dd, $J = 8.0, 1.8$ Hz, 1H), 8.30 (Ar-H, ddd, $J = 12.0, 8.0, 1.4$ Hz, 2H), 7.79–7.65 (Ar-H, m, 2H), 7.04 (Ar-H, dd, $J = 8.0, 4.0$ Hz, 1H), 6.81 (Ar-H, m, 2H), 1.94 (CH_3 , 2H, s). ^{13}C NMR (101 MHz, DMSO- d_6) δ_{C} 161.6 (C), 151.98, 143.1, 137.7, 137.1, 137.0,



Scheme 1 Synthesis of N-benzylquinoline-8-sulfonamide (**a1–18**).

136.2, 134.8, 132.2, 132.2, 131.9, 129.0, 128.4, 128.3, 126.2, 123.3, 112.5, 112.4, 110.9, 110.7 (Ar C), 17.28 (CH₂). Anal. calculated for C₁₇H₁₅FN₂O₂S, %: C, 61.80; H, 4.58; N, 8.48; found, %: C, 61.84; H, 4.60; N, 8.52.

3.1.3 *N*-(2,6-Difluorophenyl)quinoline-8-sulfonamide (a3). Yield 80%, dark brown powder, *R*_f 0.4, (*n*-hexane/ethyl acetate: 2 : 3), M.P: 254–257 °C, FTIR (ν cm⁻¹), 3211 (stretching, NH), 1682 (stretching, C=C), 1356 (stretching, S:O), 712 (stretching, CF), cm⁻¹. ¹H NMR (400 MHz, DMSO-*d*₆) δ 9.67 (NH, 1H, brs), 9.09 (Ar-H, dd, *J* = 4.0, 1.8 Hz, 1H), 8.65 (Ar-H, dd, *J* = 8.0, 1.8 Hz, 1H), 8.30 (Ar-H, dd, *J* = 8.0, 1.4 Hz, 1H), 8.20 (Ar-H, dd, *J* = 8.0, 1.6 Hz, 1H), 7.74 (Ar-H, dd, *J* = 8.0, 4.0 Hz, 1H), 7.68 (Ar-H, app t, *J* = 8.0, 1H), 7.20–7.05 (Ar-H, 2H, m), 6.98–6.88 (Ar-H, 1H, m). ¹³C NMR (100 MHz, DMSO) δ 161.5/161.4/158.9, 158.0/157.9/155.5/115.4, 151.8, 143.2, 137.5, 136.3, 134.7, 131.5, 129.10/129.01/128.98, 128.94, 128.9, 126.0, 123.1, 121.80/121.76/121.67/121.63, 112.02/111.98/111.80/111.76 (ArC), 105.07/104.83/104.90/104.59. Anal. calculated for C₁₅H₁₀F₂N₂O₂S, %: C, 56.25; H, 3.15; N, 8.75; found, %: C, 56.29; H, 3.18; N, 8.67.

3.1.4 *N*-(4-Chlorobenzyl)quinoline-8-sulfonamide (a4). Yield 87%, dark brownish powder, *R*_f 0.5, (*n*-hexane/ethylacetate: 2 : 3), M.P: 258–260 °C, FTIR (ν cm⁻¹), 3209 (stretching, NH), 1674 (stretching, C=C), 1325 (stretching, S:O), 781 (stretching C–Cl) ¹H NMR (400 MHz, DMSO-*d*₆) δ 9.03 (Ar-H, dd, *J* = 4.2, 1.8 Hz, 1H), 8.47 (Ar-H, dd, *J* = 8.3, 1.8 Hz, 1H), 8.21 (Ar-H, m, 2H), 7.81 (NH, t, *J* = 6.5 Hz, 1H), 7.67 (Ar-H, m, 2H), 7.05 (Ar-H, d, *J* = 8.6 Hz, 2H), 7.00 (Ar-H, d, *J* = 8.6, 2H), 4.08 (CH₂, d, *J* = 6.5 Hz, 2H). ¹³C NMR (100 MHz, DMSO) δ 151.6, 143.0, 137.4, 137.3, 136.9, 133.8, 131.8, 131.0, 129.8, 128.8, 127.8, 126.0, 122.9 (Ar-C), 46.4 (CH₂). Calculated for C₁₆H₁₃ClN₂O₂S, %: C, 57.74; H, 3.94; N, 8.42; found, %: C, 57.85; H, 3.61; N, 8.70.

3.1.5 *N*-(3-Chlorobenzyl)quinoline-8-sulfonamide (a5). Yield 87%, dark brown powder, *R*_f 0.5, (*n*-hexane/ethylacetate: 2 : 3), M.P: 256–258 °C, FTIR (ν cm⁻¹), 3209 (stretching, NH), 1674 (stretching, C=C), 1325 (stretching, S:O), 781 (stretching C–Cl) cm⁻¹. ¹H NMR (400 MHz, DMSO-*d*₆) δ 9.05 (Ar-H, dd, *J* = 4.0, 1.8 Hz, 1H), 8.47 (Ar-H, dd, *J* = 8.0, 1.8 Hz, 1H), 8.24–8.14 (Ar-H, 2H, m), 7.89 (HN, app t, *J* = 6.6, 1.4 Hz, 1H), 7.70–7.63 (Ar-H, 2H, m), 7.07 (Ar-H, app q, *J* = 4.0 Hz, 1H), 7.03–6.98 (Ar-H, 3H, m), 4.13 (CH₂, d, *J* = 4.0 Hz, 2H). ¹³C NMR (100 MHz, DMSO) δ 151.6, 142.9, 140.4, 137.4, 137.3, 133.9, 132.9, 130.8, 129.8, 128.8, 127.8, 127.1, 126.6, 125.9, 122.8 (Ar-C), 46.42 (CH₂). Anal. calculated for C₁₆H₁₃ClN₂O₂S, %: C, 57.74; H, 3.94; N, 8.42; found, %: C, 57.85; H, 3.61; N, 8.70.

3.1.6 *N*-(3,4-Dimethoxybenzyl)quinoline-8-sulfonamide (a6). Yield 89%, off white powder, *R*_f 0.3, (*n*-hexane/ethyl acetate: 2 : 3), M.P: 260–263 °C, FTIR (ν cm⁻¹), 3402 (stretching, NH), 2932 (stretching, CH), 1693 (stretching, C=C), 1373 (stretching, S:O), 1176 (stretching, C–O), 738 (stretching, C–F) cm⁻¹. ¹H NMR (400 MHz, DMSO-*d*₆) δ 9.00 (Ar-H, dd, *J* = 4.0, 1.7 Hz, 1H), 8.44 (Ar-H, dd, *J* = 8.0, 1.7 Hz, 1H), 8.21–8.10 (Ar-H, 2H, m), 7.71–7.59 (Ar-H, 2H, m), 7.05 (NH, app t, *J* = 8.0 Hz, 1H), 6.75 (Ar-H, d, *J* = 8.0, 1.5 Hz, 1H), 6.04–5.91 (Ar-H, 2H, m), 3.97 (2H, d, *J* = 8.0 Hz), 3.57 (CH₃, 3H, s), 3.41 (CH₃, 3H, s). ¹³C NMR (100 MHz, DMSO) δ 160.2, 157.7, 151.4, 142.8,

137.3, 136.8, 133.7, 130.5, 130.3, 128.7, 125.9, 122.7, 116.4, 103.9, 97.5 (Ar-C), 55.5 (OCH₃), 55.3 (OCH₃), 43.13 (CH₂). Anal. calculated for C₁₈H₁₈N₂O₄S, %: C, 60.32; H, 5.06; N, 7.82; found, %: C, 60.58; H, 5.01; N, 7.62.

3.1.7 *N*-(2,3-Dihydro-1H-benzo[d]imidazole-2-yl)quinoline-8-sulfonamide (a7). Yield 82%, cream color powder, *R*_f 0.4, (*n*-hexane/ethyl acetate: 3 : 2), M.P: 257–259 °C, ¹H NMR (400 MHz, DMSO-*d*₆) δ 1H NMR (400 MHz, DMSO-*d*₆) δ 9.21 (NH, d, *J* = 4.0 Hz, 1H), 9.02 (NH, d, *J* = 8.0 Hz, 1H), 8.94–8.88 (Ar-H, m, 1H), 8.80–8.73 (Ar-H, m, 1H), 8.52 (Ar-H, dd, *J* = 8.0, 1.5 Hz, 1H), 8.45–8.36 (Ar-H, m, 2H), 8.29 (Ar-H, d, *J* = 8.0 Hz, 1H), 7.97 (Ar-H, dd, *J* = 8.0, 5.2 Hz, 1H), 7.91–7.83 (Ar-H, m, 2H), 7.68 (dd, *J* = 8.4, 4.2 Hz, 1H), 7.34 (d, *J* = 7.4 Hz, 2H), 7.09 (d, *J* = 7.6 Hz, 1H), 6.86 (t, *J* = 7.4 Hz, 1H, CH). ¹³C NMR (101 MHz, DMSO) δ 154.1, 152.3, 143.1, 137.8, 136.8, 133.9, 133.4, 131.2, 128.9, 126.3, 124.5, 123.7, 122.5, 120.6, 116.0, 112.1.

3.1.8 *N*-(4-Iodophenyl)quinoline-8-sulfonamide (a8). Yield 84%, dark brown powder, *R*_f 0.4, (*n*-hexane/ethyl acetate: 2 : 3), M.P: 260–262 °C, FTIR (ν cm⁻¹), 2964 (stretching, NH), 1634 (stretching C=C), 1342 (stretching, S:O), 681 (stretching, C–F) cm⁻¹. ¹H NMR (400 MHz, DMSO-*d*₆) δ 10.29 (NH, 1H, brs), 9.11 (Ar-H, dd, *J* = 4.0, 1.8 Hz, 1H), 8.51 (Ar-H, dd, *J* = 8.0, 4.0 Hz, 1H), 8.36 (Ar-H, dd, *J* = 8.0, 1.4 Hz, 1H), 8.27 (Ar-H, dd, *J* = 8.0, 1.4 Hz, 1H), 7.73–7.69 (Ar-H, 2H, m), 7.46–7.38 (Ar-H, 2H, m), 7.41 (Ar-H, d, *J* = 8.0 Hz, 1H). ¹³C NMR (101 MHz, DMSO) δ 151.9 (C), 143.1, 138.2, 137.9, 137.5, 135.3, 134.9, 132.8, 128.9, 126.1, 123.2, 122.0, 88.1 (Ar-C). Anal. calculated for C₁₅H₁₁IN₂O₂S, %: C, 43.92; H, 2.70; N, 6.83; found, %: C, 43.72; H, 2.51; N, 6.55.

3.1.9 *N*-(4-Cyanophenyl)quinoline-8-sulfonamide (a9). Yield 89%, cream color powder, *R*_f 0.4, (*n*-hexane/ethyl acetate: 2 : 3), M.P: 257–259 °C, FTIR (ν cm⁻¹), 3296 (stretching, NH), 2266 (stretching, CN), 1649 (stretching, C=C), 1344 (stretching, S:O), 681 (stretching, C–F) cm⁻¹. ¹H NMR (400 MHz, DMSO-*d*₆) δ 10.98 (NH, 1H, brs), 9.09 (Ar-H, dd, *J* = 4.0, 1.8 Hz, 1H), 8.50 (Ar-H, td, *J* = 8.0, 2.4 Hz, 2H), 8.30 (Ar-H, d, *J* = 8.0 Hz, 1H), 7.76 (Ar-H, t, *J* = 8.0 Hz, 1H), 7.69 (Ar-H, dd, *J* = 8.0, 4.0 Hz, 1H), 7.57 (Ar-H, d, *J* = 8.0 Hz, 2H), 7.23 (Ar-H, d, *J* = 8.0 Hz, 2H). ¹³C NMR (101 MHz, DMSO) δ 152.1 (C), 143.1, 142.9, 137.5, 135.3, 135.2, 133.8, 133.1, 128.9, 126.2, 123.2, 119.2, 118.6, 105.3 (Ar-C). Anal. calculated for C₁₆H₁₁N₃O₂S, %: C, 62.12; H, 3.58; N, 13.58; found, %: C, 62.36; H, 3.31; N, 13.38.

3.1.10 *N*-(Cyclohexylmethyl)quinoline-8-sulfonamide (a10). Yield 81%, color: light yellow powder, *R*_f 0.3, (*n*-hexane/ethyl acetate: 2 : 3), M.P: 264–266 °C, FTIR (ν cm⁻¹), 3373 (NH, stretching), 1625 (stretching, C=C), 1348 (stretching, S:O), cm⁻¹. ¹H NMR (400 MHz, DMSO-*d*₆) δ 9.07 (Ar-H, dd, *J* = 4.0, 1.4 Hz, 1H), 8.55 (Ar-H, dd, *J* = 8.4, 4.0 Hz, 1H), 8.30 (Ar-H, d, *J* = 8.0 Hz, 1H), 7.79–7.68 (Ar-H, 2H, m), 7.14 (NH, 1H, app t, *J* = 8.0 Hz), 2.58 (CH₂, t, *J* = 8.0 Hz, 2H), 1.55–1.49 (cyclohexyl-H, 5H, m), 1.27 (cyclohexyl-H, 1H, m), 1.02–0.93 (cyclohexyl-H, 3H, m), 0.74–0.64 (cyclohexyl-H, 2H, m). ¹³C NMR (101 MHz, DMSO) δ 151.8 (C), 143.1, 137.6, 136.8, 134.0, 131.1, 128.9, 126.2, 123.0, 49.5, 40.6, 40.4, 40.2, 39.9, 39.8, 39.6, 39.3, 37.6, 30.6, 26.3, 25.7. Anal. calculated for C₁₆H₂₀N₂O₂S, %: C, 63.13; H, 6.62; N, 9.20; found, %: C, 63.43; H, 6.40; N, 9.30.



3.1.11 N-(2-Hydroxyphenyl)quinoline-8-sulfonamide (a11).

Yield 84%, dark brown powder, R_f : 0.5, (*n*-hexane/ethyl acetate: 2 : 3), M.P.: 260–263 °C, FTIR (ν cm⁻¹), 3458 (stretching, OH), 3174 (stretching, NH), 1570 (stretching, C=C), 1267 (stretching, S:O) cm⁻¹. ¹H NMR (400 MHz, DMSO-*d*₆) δ_H 9.94 (NH, 1H, brs), 9.31 (OH, 1H, brs), 9.13 (Ar-H, dd, J = 4.0, 1.8 Hz, 1H), 8.51 (Ar-H, dd, J = 8.0, 1.8 Hz, 1H), 8.34 (Ar-H, dd, J = 8.0, 1.4 Hz, 1H), 8.26 (Ar-H, dd, J = 8.0, 1.5 Hz, 1H), 7.73–7.69 (Ar-H, m, 2H), 6.83 (Ar-H, t, J = 8.0 Hz, 1H), 6.51 (Ar-H, app t, J = 1.6 Hz, 1H), 6.47 (Ar-H, dd, J = 8.0, 0.8 Hz, 1H), 6.51 (Ar-H, app t, J = 8.0, 1.2 Hz, 1H). ¹³C NMR (101 MHz, DMSO) δ_C 158.0 (C), 151.9, 143.2, 139.3, 137.4, 135.7, 134.6, 132.5, 129.9, 128.9, 126.1, 123.1, 111.2, 110.8, 107.2 (Ar-C).

3.1.12 N-(4-Florobenzyl)-8-quinolinesulfonamide (a12).

Yield 92%, color yellowish powder, R_f : 0.5, (*n*-hexane/ethyl acetate 2 : 3), M.P.: 260–262 °C, FTIR (ν cm⁻¹), 3262 (stretching, NH), 1586 (stretching, C=C), 1324 (stretching, S:O) cm⁻¹. ¹H NMR (400 MHz, DMSO-*d*₆) δ_H , 9.11, (dd, J = 4.23, 1.79, 1H), 8.51, (dd, J = 8.40, 1.79 Hz) 8.36, (dd, J = 7.33, 1.44 Hz, 1H), 8.27, (dd, J = 8.29, 1.42), 7.81, (t, J = 6.48, 1H), 7.71, (m, 2H), 7.42 (d, J = 8.79, 2H), 6.87, (d, J = 8.43 Hz, 2H), 4.09 (d, J = 6.53 Hz, 2H). ¹³C NMR (100 MHz, DMSO) δ_C 151.8, 142.8, 142.7, 137.3, 135.0, 134.9, 133.6, 132.9, 128.7, 125.9, 123.0, 119.0, 118.4 (Ar-Cs), 47.6 (CH₂).

3.1.13 N-(2-Fluorobenzyl)quinoline-8-sulfonamide (a13).

Yield 81%, light yellow powder, R_f : 0.5, (*n*-hexane/ethyl acetate: 2 : 3), M.P.: 250–252 °C, FTIR (ν cm⁻¹), 3411 (stretching, NH), 2954 (stretching, CH), 1687 (stretching, C=C), 1367 (stretching, S:O), 703 (stretching, C-F). ¹H NMR (400 MHz, DMSO-*d*₆) δ_H 9.03 (Ar-H, app dd, J = 4.0, 1.8 Hz, 1H), 8.47 (Ar-H, dd, J = 8.0, 1.8 Hz, 1H), 8.25–8.16 (Ar-H, 2H, m), 7.81 (NH, app t, J = 6.0 Hz, 1H), 7.72–7.61 (Ar-H, 2H, m), 7.09–6.96 (Ar-H, 4H, m), 4.08 (CH₂, d, J = 6.0 1.4 Hz, 2H), ¹³C NMR (101 MHz, DMSO) δ_C 151.6, 143.0, 137.34/137.28, 136.9, 133.8, 131.8, 130.9, 129.8, 128.8, 127.8, 126.0, 122.8 (Ar-C), 46.4 (CH₂). Anal. calculated for C₁₆H₁₃FN₂O₂S, %: C, 60.75; H, 4.14; N, 8.86; found, %: C, 60.88; H, 4.34; N, 8.95.

3.1.14 N-(3-Fluoro-5-(trifluoromethyl)benzyl)quinoline-8-sulfonamide (a14). Yield 91%, cream powder, R_f : 0.5, (*n*-hexane/ethyl acetate: 2 : 3), M.P.: 258–260 °C, FTIR (ν cm⁻¹), 3282 (stretching, NH), 1658 (stretching, C=C), 1334 (stretching, S:O), 746 (stretching, C-F) cm⁻¹. ¹H NMR (400 MHz, DMSO-*d*₆) δ_H 9.03 (Ar-H, dd, J = 4.0, 1.8 Hz, 1H), 8.47 (Ar-H, dd, J = 8.0, 1.8 Hz, 1H), 8.21 (Ar-H, dd, J = 8.0, 1.4 Hz, 2H), 7.78 (NH, app t, J = 8.0 Hz, 1H), 7.69–7.64 (Ar-H, 2H, m), 7.06 (Ar-H, dd, J = 8.0, 3.2 Hz, 2H), 6.65 (Ar-H, app t, J = 8.0 Hz, 2H), 4.08 (Ar-H, d, J = 8.0 Hz, 2H). ¹³C NMR (101 MHz, DMSO) δ 160.2/160.2, 151.6, 142.9, 137.4/137.3, 133.8, 130.8, 129.99/129.91, 128.8, 126.0, 122.9, 114.7/114.5 (Ar-C), 46.4 (CH₂). Anal. calculated for C₁₆H₁₃ClN₂O₂S, %: C, 53.13; H, 3.15; N, 7.29; found, %: C, 53.28; H, 3.43; N, 7.48.

3.1.15 N-(2,4-Dichlorobenzyl)-8-quinolinesulfonamide (a15). Yield 81%, color brownish, R_f : 0.4, (*n*-hexane/ethyl acetate 2 : 3), M.P.: 264–266 °C, FTIR (ν cm⁻¹), 3273 (stretching, NH), 1610 (stretching, C=C), 1311 (stretching, S:O) cm⁻¹. ¹H (400 MHz, DMSO-*d*₆) δ_H , 9.19 (dd, J = 4.3, 1.7 Hz, 1H, Ar-H), 8.62 (dd, J = 8.3, 1.7 Hz, 1H, Ar-H), 8.42–8.27 (m, 2H, Ar-H), 7.92–7.78 (m, 2H, Ar-H), 7.24 (t, J = 6.4 Hz, NH, 1H), 6.94 (d, J = 8.2 Hz, 1H, Ar-

H), 6.70 (m, 2H, Ar-H), 4.16 (d, J = 6.3 Hz, 2H, CH₂). ¹³C NMR (100 MHz, DMSO) δ 161.32, 158.79, 152.46, 143.93, 138.41, 137.93, 134.82, 131.65, 131.41, 129.80, 127.06, 123.84, 117.54, 105.03, 98.62 (Ar Cs), 43.15 (CH₂).

3.1.16 N-(2-Chlorobenzyl)-8-quinolinesulfonamide (a16).

Yield 84%, color light brown, R_f : 0.5, (*n*-hexane/ethyl acetate 2 : 3), M.P.: 262–263 °C, FTIR (ν cm⁻¹), 3300 (stretching, NH), 1613 (stretching, C=C), 1326 (stretching, S:O) cm⁻¹. ¹H (400 MHz, DMSO-*d*₆) δ_H , 9.28 (dd, J = 4.3, 1.8 Hz, 1H, Ar-H), 8.75 (dd, J = 8.4, 1.8 Hz, 1H, Ar-H), 8.51 (m, 2H, Ar-H), 7.92 (m, 3H, Ar-H), 7.65 (t, J = 6.55, NH 1H) 7.36 (m, 1H, Ar-H), 7.29 (dd, J = 8.1, 1.6 Hz, 1H, Ar-H), 6.99 (td, J = 7.6, 1.7 Hz, 1H, Ar-H), 4.23 (d, J = 6.52, 2H, Ar-H). ¹H NMR (400 MHz, DMSO-*d*₆) δ 9.28 (dd, J = 4.3, 1.8 Hz, 1H), 8.75 (dd, J = 8.4, 1.8 Hz, 1H), 8.51 (m, 2H), 7.92 (m, 3H), 7.65 (t, J = 6.55, 1H) 7.36 (m, 1H), 7.29 (dd, J = 8.1, 1.6 Hz, 1H), 6.99 (td, J = 7.6, 1.7 Hz, 1H), 4.23 (d, J = 6.52, 2H). ¹³C NMR (100 MHz, DMSO) δ 152.24, 142.84, 139.96, 138.92, 137.75, 135.76, 134.94, 133.80, 131.68, 129.52, 129.02, 127.49, 126.21, 123.32, 122.69 (Ar-C), 45.89 (CH₂).

3.1.17 N-(2,5-Dichloro-4-hydroxyphenyl)quinoline-8-sulfonamide (a17). Yield 87%, dark brown powder, R_f : 0.5, (*n*-hexane/ethyl acetate: 2 : 3), M.P.: 266–268, FTIR (ν cm⁻¹), 3402 (stretching, OH), 3170 (stretching, NH), 1618 (stretching, C=C), 1361 (stretching, S:O) cm⁻¹. ¹H NMR (400 MHz, DMSO-*d*₆) δ_H , 10.13 (NH, 1H, brs), 9.89 (OH, 1H, brs), 9.14 (Ar-H, dd, J = 4.0, 1.8 Hz, 1H), 8.53 (Ar-H, dd, J = 8.0, 4.0 Hz, 1H), 8.34 (Ar-H, dd, J = 8.0, 1.4 Hz, 1H), 8.29 (Ar-H, dd, J = 8.0, 1.4 Hz, 1H), 7.75–7.70 (Ar-H, m, 2H), 6.98 (Ar-H, app s, 2H). ¹³C NMR (100 MHz, DMSO) δ_C 152.0 (C), 146.2, 143.0, 137.6, 135.1, 135.0, 132.7, 130.9, 128.8, 126.2, 123.2, 122.7, 120.9 (Ar-C).

3.1.18 N-(4-Methoxybenzyl)-8-quinolinesulfonamide (a18).

Yield 84%, color brown, R_f : 0.5, (*n*-hexane/ethyl acetate 2 : 3) M.P.: 265–268 °C, FTIR (ν cm⁻¹), 3240 (stretching, NH), 1710 (stretching, C=C), 1324 (stretching, S:O) cm⁻¹. ¹H NMR (DMSO-*d*₆) δ_H 9.03 (dd, J = 4.2, 1.8 Hz, 1H, Ar-H), 8.47 (dd, J = 8.3, 1.8 Hz, 1H), 8.21 (m, 2H, Ar-H), 7.81 (t, J = 6.5 Hz, 1H, Ar-H), 7.67 (m, 2H, Ar-H), 7.02 (m, 4H, Ar-H), 4.08 (d, J = 6.5 Hz, 2H, CH₂), 3.57 (s, 3H, CH₃). ¹³C NMR (100 MHz, DMSO) δ_C 151.58, 143.00, 137.34, 137.28, 136.92, 133.84, 131.79, 130.95, 129.76, 128.81, 127.84, 126.02, 122.87 (Ar-Cs), 58.48 (CH₂), 46.36 (CH₃).

3.2. Biological activates (*in vitro* enzyme assay)

3.2.1 Monoamine oxidase (MAO-A and MAO-B) inhibition assay. Enzyme assay was performed with previously reported protocols with slightly modified procedures, the newly synthesized compounds were tested against MAO-A and MAO-B.²⁴ The assay was performed in a white 96-well plate consisting of buffer (NaHPO₄, pH 7.4) 60 μ L, 0.1 mM of samples in (10% DMSO) 10 μ L and 26 μ g of MAO-A and 5 μ g of MAO-B were added accordingly and the mixture was incubated for 20 min for MAO-A and 15 min for MAO-B. Subsequently, substrate 3 mM, 10 μ L, and Amplex red 10 μ L were added to each well. The final volume was 100 μ L.²⁶ Positive controls for MAO-A and MAO-B, Clorgyline, and Deprenyl 10 μ L of 1 mM were used respectively. The change in fluorescence excitation 540 nm and emission 590 nm was determined through a fluorescence plate reader (BMG Labtech GmbH, Ortenberg, Germany). An IC₅₀ value was



determined for compounds that inhibit MAO-A or MAO-B above 50%. All experiments were repeated in triplicate. The non-linear curve fitting program (PRISM 5.0) was used to calculate IC_{50} values (GraphPad, San Diego, California, USA).³⁷

3.2.2 Cholinesterase (AChE and BChE) inhibition assay. An Ellmann's method with some modifications was used to determine cholinesterase activity. The assay was performed in a transparent 96-well plate consisting of buffer (KH_2PO_4 , pH 7.8) 60 μ L, samples (0.1 mM, 10% DMSO) 10 μ L and enzyme AChE (EC 3.1.17, electric eels, 2.0 U mg^{-1}) and BChE (serum of horse, 1 μ L mg^{-1}) were added accordingly and the mixture was incubated for 15 min. Afterwards, substrate acetylthiocholine chloride (ATCCL) or butyryl thiocholine chloride (BTCCL), 3 mM, 10 μ L and 5,5'-dithiobis-(2-nitrobenzoic acid) (DTNB) 0.5 mM, 10 μ L was added, allowed to incubate for 25 minutes at 37 °C, and absorbance was measured. Positive control Donepezil for AChE and BChE (0.1 mM) 10 μ L used. We used graphs pad 5.0 software (san diego, California, USA) to calculate the IC_{50} values of the compounds with more than 50% inhibition potential.³⁸

3.3. *In silico* studies

The MOE 2019 software package was used to conduct an *in silico* study on MAO-A (PDB ID: 2Z5Y), MAO-B (PDB ID: 2V5Z), AChE (PDB ID: 4BDT), and BChE (PDB ID: 4TPK). Re-docking of the cognate ligand occurred immediately after the protein was prepared.²⁶ An RMSD of 1.8 were found, indicating that the docking protocol was appropriate.³⁹ The re-docking process also showed that the ligand was in the same binding pocket as the original one. The binding affinity was found to be in a range of -7.9 to -10.76 kcal mol^{-1} . This confirmed that the docking protocol was successful and yielded the expected results.⁴⁰

3.4. Enzyme extraction

Mice livers from male albinos (between 250 and 300 g) were collected to obtain mitochondrial-enriched sections. In the first step, liver (20–30 g) was crushed into small pieces in an ice cold Hepes buffer (5.0 mM, pH 7.4) consisting of sucrose 70 mM, mannitol 210 mM, and ethylene glycol tetraacetic acid (EGTA) in a 50 mL beaker. The mixture was homogenized at 1100 rpm, and transferred into a 45 mL falcon and centrifuged at 1000 rpm for 30 min and the upper layer (supernatant) was collected and further centrifuged at 11 000 rpm for 30 min at 0 °C. repeated the same step twice. The pellet was re-suspended in 50 mM of buffer ($NaHPO_4$, pH 7.4), transferred into small Eppen doffs and stored at -80 °C until further use.³⁷

3.5. Docking protocol

3.5.1 Ligand preparation and optimization. Compound libraries of synthetic compounds were prepared and cognate ligands were taken from proteins. In the molecular operating environment (MOE 2019) the energy minimization of all structures was done using default parameters. Crystal structures of all targeted enzymes were downloaded from the Protein Data Bank (RCSB PDB). In protein preparation, initially water molecules, co-factors, and FAD were removed, and the targeted

protein was protonated by default parameters. To validate the protein, a cognitive ligand was redocked, and the results were analyzed which showed the same binding interactions as reported. With the help of site finder active site of the enzyme was determined and a library of compound was docked. After docking the lowest binding energy score poses was selected. Visualization was done by using discovery studio to find the favorable interactions.³⁹

3.6. *In silico* ADME analysis

Physicochemical and pharmacokinetic properties (Absorption, Distribution, Metabolism and Excretion) of all the compounds (**a1–18**) were assessed by SwissADME web server. The SMILES format of each synthetic derivative was obtained from Chem-Draw and put on the web server to predict the pharmacokinetic profile.³⁵

4 Conclusion

In summary, a new library of quinoline-based sulfonamide derivatives was synthesized and explored against MAO-A, MAO-B, AChE and BChE. Among them compounds **a5**, **a12**, **a11**, and **a6** were found to be the most potent having IC_{50} values of 0.59 ± 0.04 , 0.47 ± 0.03 , 0.58 ± 0.05 and 1.10 ± 0.77 μ M respectively. As compared to other enzymes, compounds with the *m*-chloro substitution displayed 2-fold enhanced potency against MAO-A. In contrast, the *o*-fluoro substitution exhibited a 2-fold higher potency against MAO-B than other enzymes. *o*-Hydroxy had a 1-fold enhanced potency toward AChE than other enzymes. The kinetic studies of the most potent compound showed competitive inhibition. In addition, *in silico* analysis revealed ligand–protein interactions such as hydrogen bonding, π -alkyl, and π -sulfur with various catalytic amino acid residues. The importance of this target in AD and PD pathogenesis suggests that these compounds may be useful for developing multitarget-directed ligands. Based on our results, compound **a5**, **a6**, **a11**, **a12**, **a15**, and **a18** is a promising “one-compound-multi-target” candidate for AD treatment and needs further study.

Author contributions

Saqib Jalil: synthesis, methodology, formal analysis, validation investigation (bioactivity), writing – original draft preparation (bioactivity part), software. Saqib Jalil and Zahid Hussain: synthesis, methodology, formal analysis, validation. Syed Mubashir Ali Abid: *in silico* studies (computational). Abdul Hameed: manuscript writing and spectral data. Jamshed Iqbal: supervision, resources (synthesis), data curation, writing–original draft reviewing and editing, supervision, resources (bioactivity and docking), funding acquisition.

Conflicts of interest

The authors declare that they have no conflict of interest.



Acknowledgements

The authors gratefully acknowledge the financial support for this research provided by the Higher Education Commission of Pakistan (HEC) via NRP Project No. 20-15846/NRP/R&D/HEC/2021, German-Pakistani Research Collaboration Programme and Equipment Grant funded by DAAD, Germany.

References

- 1 M. M. Gonzales, *et al.*, Biological aging processes underlying cognitive decline and neurodegenerative disease, *J. Clin. Invest.*, 2022, **132**(10), e158453.
- 2 E. Connell, *et al.*, Microbial-derived metabolites as a risk factor of age-related cognitive decline and dementia, *Mol. Neurodegener.*, 2022, **17**(1), 43.
- 3 M. Nasb, W. Tao and N. Chen, Alzheimer's Disease Puzzle: Delving into Pathogenesis Hypotheses, *Aging Dis.*, 2023, **15**(2), 43–73.
- 4 N. I. Bohnen, *et al.*, Recent advances in cholinergic imaging and cognitive decline—revisiting the cholinergic hypothesis of dementia, *Curr. Geriatr. Rep.*, 2018, **7**, 1–11.
- 5 N. Kumar, *et al.*, Advancements in the development of multi-target directed ligands for the treatment of Alzheimer's disease, *Bioorg. Med. Chem.*, 2022, 116742.
- 6 A. U. Syed, *et al.*, Comparison of Monoamine Oxidase-A, A β Plaques, Tau, and Translocator Protein Levels in Postmortem Human Alzheimer's Disease Brain, *Int. J. Mol. Sci.*, 2023, **24**(13), 10808.
- 7 Z.-R. Chen, *et al.*, Role of cholinergic signaling in Alzheimer's disease, *Molecules*, 2022, **27**(6), 1816.
- 8 S. Manzoor and N. Hoda, A comprehensive review of monoamine oxidase inhibitors as Anti-Alzheimer's disease agents: A review, *Eur. J. Med. Chem.*, 2020, **206**, 112787.
- 9 M. B. Youdim, Monoamine oxidase inhibitors, and iron chelators in depressive illness and neurodegenerative diseases, *J. Neural Transm.*, 2018, **125**(11), 1719–1733.
- 10 I. Vecchio, *et al.*, The state of the art on acetylcholinesterase inhibitors in the treatment of Alzheimer's disease, *J. Cent. Nerv. Syst. Dis.*, 2021, **13**, 11795735211029113.
- 11 B. S. Matada, R. Pattanashettar and N. G. Yernale, A comprehensive review on the biological interest of quinoline and its derivatives, *Bioorg. Med. Chem.*, 2021, **32**, 115973.
- 12 D. J. Kucharski, M. K. Jaszczak and P. Boratyński, A review of modifications of quinoline antimalarials: mefloquine and (hydroxy) chloroquine, *Molecules*, 2022, **27**(3), 1003.
- 13 K. B. Patel and P. Kumari, A review: Structure-activity relationship and antibacterial activities of Quinoline based hybrids, *J. Mol. Struct.*, 2022, **1268**, 133634.
- 14 T.-H. Qin, *et al.*, Synthesis and biological evaluation of new 2-substituted-4-amino-quinolines and-quinazoline as potential antifungal agents, *Bioorg. Med. Chem. Lett.*, 2022, **72**, 128877.
- 15 M. Jeleń, B. Morak-Młodawska and R. Korlacki, Anticancer activities of tetra-, penta-, and hexacyclic phenothiazines modified with quinoline moiety, *Mol. Struct.*, 2023, 135700.
- 16 H. B. Shivaji and K. R. Rajendra, Structure based drug discovery, docking modelling, synthesis and anticonvulsant pharmacological activity of new quinoline derivatives, *Int. J. Health Sci.*, 2022, (II), 9534–9548.
- 17 A. M. Ghanim, *et al.*, Design and synthesis of ibuprofen-quinoline conjugates as potential anti-inflammatory and analgesic drug candidates, *Bioorg. Chem.*, 2022, **119**, 105557.
- 18 V. Snehi, *et al.*, An Extensive Review on Biological Interest of Quinoline and Its Analogues, *Int. J. Sci. Healthcare Res.*, 2023, **8**, 45–66.
- 19 M. S. S. Chauhan, T. Umar and M. K. Aulakh, Quinolines: Privileged Scaffolds for Developing New Anti-neurodegenerative Agents, *ChemistrySelect*, 2023, **8**(14), e202204960.
- 20 A. Marella, *et al.*, Quinoline: A versatile heterocyclic, *Saudi Pharm. J.*, 2013, **21**(1), 1–12.
- 21 A. Irfan, *et al.*, Coumarin sulfonamide derivatives: An emerging class of therapeutic agents, *Heterocycl. Commun.*, 2020, **26**(1), 46–59.
- 22 B. Mavroidi, *et al.*, The prophylactic and multimodal activity of two isatin thiosemicarbazones against Alzheimer's disease in vitro, *Brain Sci.*, 2022, **12**(6), 806.
- 23 S. Kumar, *et al.*, Exploration of the detailed structure–activity relationships of isatin and their isomers as monoamine oxidase inhibitors, *ACS Omega*, 2022, **7**(19), 16244–16259.
- 24 A. A. Shetnev, *et al.*, Investigation of Novel Thiazole Derivatives Bearing the Benzenesulfonamide Moiety as MAO Inhibitors with a Promising Activity Profiles. Preprint, 2023.
- 25 Z. H. Li, L. Q. Yin, D. H. Zhao, L. H. Jin, Y. J. Sun and C. Tan, SAR studies of quinoline and derivatives as potential treatments for Alzheimer's disease, *Arabian J. Chem.*, 2023, **16**(2), 104502.
- 26 H. Chen, *et al.*, Design, synthesis and evaluation of quinoline-O-carbamate derivatives as multifunctional agents for the treatment of Alzheimer's disease, *J. Enzyme Inhib. Med. Chem.*, 2023, **38**(1), 2169682.
- 27 M. B. Rosenthal, Novel Alzheimer disease treatments and reconsideration of us pharmaceutical reimbursement policy, *J. Am. Med. Assoc.*, 2023, **303**(6), 505–506.
- 28 M. M. Martins, P. S. Branco and L. M. Ferreira, Enhancing the Therapeutic Effect in Alzheimer's Disease Drugs: The role of Polypharmacology and Cholinesterase inhibitors, *ChemistrySelect*, 2023, **8**(10), e202300461.
- 29 A. A. Njan, *et al.*, Identification of neurotherapeutic constituents in *Ocimum gratissimum* with cholinesterase and mono amine oxidase inhibitory activities, using GC-MS analysis, in vitro, and in silico approaches, *Inf. Med. Unlocked*, 2023, 101261.
- 30 Q.-H. Jin, *et al.*, (S)-N-Benzyl-1-phenyl-3, 4-dihydroisoquinoline-2 (1 H)-carboxamide Derivatives, Multi-Target Inhibitors of Monoamine Oxidase and Cholinesterase: Design, Synthesis, and Biological Activity, *Molecules*, 2023, **28**(4), 1654.
- 31 K. Jangid, *et al.*, Virtual screening and molecular dynamics simulation approach for the identification of potential multi-target directed ligands for the treatment of Alzheimer's disease, *J. Biomol. Struct. Dyn.*, 2023, 1–19.



- 32 S. Kumar and S. R. Ayyannan, Identification of new small molecule monoamine oxidase-B inhibitors through pharmacophore-based virtual screening, molecular docking and molecular dynamics simulation studies, *J. Biomol. Struct. Dyn.*, 2022, 1–22.
- 33 A. Daina, O. Michielin and V. Zoete, SwissADME: a free web tool to evaluate pharmacokinetics, drug-likeness and medicinal chemistry friendliness of small molecules, *Sci. Rep.*, 2017, 7(1), 42717.
- 34 A. Daina and V. Zoete, A boiled-egg to predict gastrointestinal absorption and brain penetration of small molecules, *ChemMedChem*, 2016, 11(11), 1117–1121.
- 35 C. A. Lipinski, *et al.*, Experimental and computational approaches to estimate solubility and permeability in drug discovery and development settings, *Adv. Drug Delivery Rev.*, 1997, 23(1–3), 3–25.
- 36 J. B. Baell and G. A. Holloway, New substructure filters for removal of pan assay interference compounds (PAINS) from screening libraries and for their exclusion in bioassays, *J. Med. Chem.*, 2010, 53(7), 2719–2740.
- 37 N. T. Tzvetkov, *et al.*, Indazole- and Indole-5-carboxamides: Selective and Reversible Monoamine Oxidase B Inhibitors with Subnanomolar Potency, *J. Med. Chem.*, 2014, 57(15), 6679–6703.
- 38 P. George and M. Abernethy, Improved Ellman procedure for erythrocyte cholinesterase, *Clin. Chem.*, 1983, 29(2), 365–368.
- 39 N. T. Tzvetkov, *et al.*, Indazole-and indole-5-carboxamides: Selective and reversible monoamine oxidase B inhibitors with subnanomolar potency, *J. Med. Chem.*, 2014, 57(15), 6679–6703.
- 40 P. C. Tomy and C. G. Mohan, Chemical space navigation by machine learning models for discovering selective MAO-B enzyme inhibitors for Parkinson's disease, *Artif. Intell. Chem.*, 2023, 1(2), 100012.

